Available online at www.sciencedirect.com
SCIENCE DIRECT®

Journal of the European Ceramic Society 23 (2003) 1549–1558
www.elsevier.com/locate/jeurceramsoc

Screen printing of co-precipitated $NiMn_2O_{4+\delta}$ for production of NTCR thermistors

R. Schmidt[a,*], A. Stiegelschmitt[b], A. Roosen[b], A.W. Brinkman[a]

[a]*Department of Physics, University of Durham, South Road, Durham DH1 3LE, UK*
[b]*University of Erlangen-Nuremberg, Department of Materials Science, Glass and Ceramics, Martenstr.5, 91058 Erlangen, Germany*

Received 28 June 2002; received in revised form 7 October 2002; accepted 19 October 2002

Abstract

Screen printing and sintering procedures have been established to produce ~25 μm thick, uniform ceramic $NiMn_2O_{4+\delta}$ films on alumina (thick film grade) substrates. $NiMn_2O_{4+\delta}$ source powder was prepared by calcination of $NiMn_2(C_2O_4)_3{\cdot}6\ H_2O$ co-precipitated from nickel and manganese oxalate precursor solutions of precisely determined concentration (by titration methods). Decomposition of $NiMn_2(C_2O_4)_3{\cdot}6\ H_2O$ into its constituent oxides in air was found to take place at ~300 °C using thermal gravimetric analysis. Formation of phase pure $NiMn_2O_{4+\delta}$ occurred at temperatures above 800 °C and was accompanied by a significant increase in grain size. At constant temperature grain growth displayed an approximately linear dependence on time. Heating the precursor to 850 °C for 30 min was found to be near the optimum, ensuring that the reaction had gone to completion while simultaneously minimising grain growth. Two types of film were fabricated; one in which the source $NiMn_2O_{4+\delta}$ powder was only mixed with organic binders and a second set to which a glass phase and a dispersing agent had been added as well. Printed films were sintered at 850 °C for 30 min. Films with the added glass phase were found by SEM and laser profileometry to have superior morphology and to be denser than films without glass. Resistance vs. temperature (R–T) characteristics were measured over the temperature range 122 K –345 K and indicated that conduction was well described by a variable - range - hopping model, in which electron transfer takes place between Mn^{3+} and Mn^{4+} cations. Films containing the glass phase were found to be slightly more resistive and marginally less temperature sensitive.

Keywords: Co-precipitation; Grain growth; $NiMn_2O_4$; Oxalates; Screen-printing; Thermistors

1. Introduction

$NiMn_2O_{4+\delta}$ ceramics are typical spinel type NTCR thermistor materials where the oxygen atoms form a cubic closed packed formation. In regular spinels divalent cations are located on tetrahedral lattice interstices and trivalent cations on octahedral sites. However, $NiMn_2O_{4+\delta}$ is not a regular spinel but has a degree of inversion, which means that some divalent nickel cations move from tetrahedral to octahedral sites. Trivalent manganese cations on octahedral sites disproportionate to Mn^{2+} and Mn^{4+} and the Mn^{2+} cations move to the tetrahedral sites to compensate the Ni^{2+} vacancies.[1] For electric conduction electron transfer takes place only between Mn^{3+} and Mn^{4+} cations on neighbouring octahedral lattice sites.[2] The electron transfer can be treated as conduction between localised electron states, is thermally activated and displays a negative temperature coefficient (NTCR) behaviour where the resistance decreases logarithmically with increasing temperature. This makes the compound well suited for temperature sensing applications.

In bulk material there are often problems with poor stability and reproducibility due to high porosity and incomplete intergranular contact. In principle, these difficulties can be minimised in films and in previous communications we have shown that thin films of $NiMn_2O_{4+\delta}$ can be grown via electron-beam evaporation.[3,4] However, $NiMn_2O_{4+\delta}$ is a complex ternary compound and physical vapour deposition without loss of stoichiometry proved to be difficult. Consequently, screen-printing procedures have been established as a direct deposition technique. The quality of screen-printed films is critically dependent on the properties of the

* Corresponding author.

0955-2219/03/$ - see front matter
PII: S0955-2219(02)00414-4

screen-printing paste, in particular the rheological behaviour and homogeneity. In turn these are functions of the added dispersing and binding agents and the particle size of the source powder. This paper reports on the preparation of optimum small average grain size $NiMn_2O_{4+\delta}$ powder, the optimisation of the printing paste and the effects of the paste components on the structure and the R–T characteristics of the resulting thick films. The optimisation of the printing and the sintering procedures is described as well.

2. Experimental details

2.1. Synthesis of $NiMn_2O_{4+\delta}$ spinel powder

The preparation of $NiMn_2O_{4+\delta}$ has been described briefly in an earlier publication but will be described in full here.[5]

$NiMn_2O_{4?\delta}$ was produced via the thermal decomposition of co-precipitated nickel manganese oxalate $NiMn_2(C_2O_4)_3{\cdot}6\ H_2O$ as described by Feltz et al.[6,7] Note this compound has the required 1:2 nickel–manganese ratio appropriate for forming homogeneous $NiMn_2O_{4+\delta}$ powder. The $NiMn_2(C_2O_4)_3{\cdot}6\ H_2O$ compound guarantees an intimate mix of nickel and manganese atoms and can be thermally decomposed at temperatures of $\sim$800 °C resulting in a powder with a small average grain size distribution. The more conventional procedure of firing precursor oxides of the NiO-Mn_2O_3 system requires higher temperatures resulting in problems due to phase transitions over 1150 °C as indicated in the phase diagram given by Wickham.[8]

The oxygen content of $NiMn_2O_{4+\delta}$ depends on the sintering history of the particular specimen. All specimens described in the results presented here had exactly the same sintering treatment, so δ is regarded as being constant throughout this work.

The co-precipitation production route is depicted in Fig. 1. Three different stock solutions containing nickel, manganese and oxalate ions were produced. The nickel stock solution was prepared by the dissolution of nickel carbonate tetra-hydrate ($NiCO_3{\cdot}4\ H_2O$) in diluted acetic acid (10%). Aqueous solutions of manganese(II) acetate tetra-hydrate [$Mn(CH_3COO)_2{\cdot}4\ H_2O$] and oxalic acid di-hydrate ($H_2C_2O_4{\cdot}2\ H_2O$) were used for the manganese and oxalate stock solutions. The concentrations of the nickel and the oxalate stock solutions were determined precisely by titration methods.

The nickel titration was carried out by forming a nickel–amine complex $[Ni(NH_3)_6]^{2+}$. Ammonium hydroxide solution (NH_4OH) was added to a precisely known amount of a few millilitres of nickel solution. The solution was further diluted and the titration carried out with Titriplex III (Na_2–EDTA) titration solution using murexide as an indicator. The concentration of the titration solution had been checked by titrating a nickel standard solution of well-known concentration.

The oxalate titration was carried out in a sulphuric acid environment at 80 °C using potassium permanganate titration solution ($KMnO_4$) without an additional indicator. The concentration of the titration solution was checked by titrating a sodium oxalate $Na_2(C_2O_4)$ standard solution. Sodium oxalate powder has no water of hydration, so solutions of precise concentration can be produced as reference solutions.

Manganese titrations turned out to be not reproducible. Therefore, the amount of water of hydration of the manganese acetate [$Mn(CH_3COO)_2{\cdot}4\ H_2O$] was determined as precisely as possible by thermal decomposition at 1200 °C and weighing the original and the resulting powder, the latter being Mn_3O_4. The thermal decomposition was carried out five times and the mean value gave 3.96 H_2O water of hydration leading to the chemical formula $Mn(CH_3COO)_2{\cdot}3.96\ H_2O$. The required quantity of manganese acetate $Mn(CH_3COO)_2{\cdot}3.96\ H_2O$ was then weighed accurately and dissolved in water.

The nickel, manganese and oxalate stock solutions of well-known concentrations were mixed together in the appropriate ratio. After 24 h the precipitation of $NiMn_2(C_2O_4)_3{\cdot}6\ H_2O$ was expected to be complete and the remaining solution was evaporated using an evacuated rotating evaporator (Heidolph, VV 2000) at 60 °C and 60 mbar. These conditions were appropriate for the evaporation of H_2O as well as organic impurities.

2.2. Optimisation of synthesized $NiMn_2O_{4+\delta}$ powder

The calcination process of $NiMn_2(C_2O_4)_3{\cdot}6\ H_2O$ leading to $NiMn_2O_{4+\delta}$, was examined by thermal gravimetric analysis (TG) in order to determine the temperature regions where decomposition reactions occur (Netzsch, Model STA 409). Exothermic and endothermic reactions were identified by differential thermal analysis (DTA).

For the printing paste a complete deagglomerated fine-grained powder is required and in order to restrict grain growth the heat exposure of the powder during the calcination process had to be minimised. This was achieved by increasing the temperature much faster in temperature regions where no reactions occurred according to the gravimetric analysis data. The heat exposure and the grain growth could be minimised effectively in this way.

To determine the optimum firing process resulting in a minimum average grain size distribution, the grain size distributions of decomposed $NiMn_2(C_2O_4)_3{\cdot}6\ H_2O$ powders fired at different temperatures for varying time periods were determined by laser granulometric measurements (Cilas, type 715). Finally, to further decrease the average grain size the calcined powder was milled in a tungsten-carbide ball mill (Retsch, model MM2000).

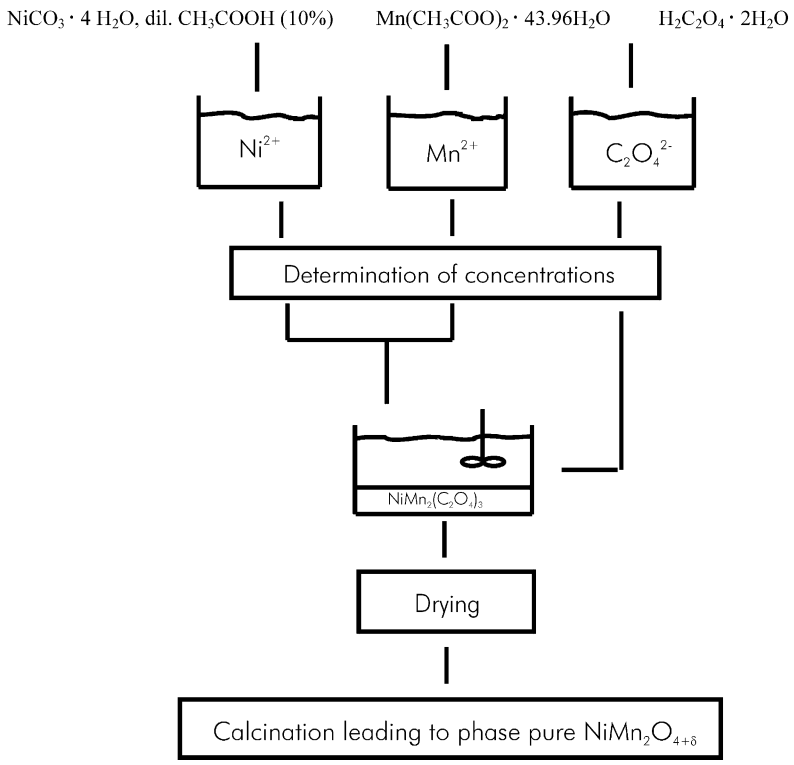

Fig. 1. Principle of the mixed oxalate route for the synthesis of $NiMn_2O_{4+\delta}$.

The minimum heat exposure was limited by the need to ensure complete formation of $NiMn_2O_{4+\delta}$ during calcination. The formation of $NiMn_2O_{4+\delta}$ was taken to be complete when no detectable precursor manganese or nickel oxide peaks were observed in the XRD (Siemens, 5000 XRD) pattern.

The stoichiometry of the optimised $NiMn_2O_{4+\delta}$ powder was assessed using Inductive Coupled Plasma spectroscopy (ICP) (Spectro Analytical Instruments, Spectroflame). For the ICP measurements the $NiMn_2O_{4+\delta}$ powder was dissolved in concentrated HCl and diluted after dissolution. The dissolving process took 24 h. Dissolution in diluted HCl or HNO_3 did not succeed.

2.3. Screen printing

In order to produce an optimum printing paste, resulting in dense and even $NiMn_2O_{4+\delta}$ films, several components had to be added to the optimised powder. Two types of printing pastes were investigated. In one, the paste was produced by mixing the $NiMn_2O_{4+\delta}$ powder with a vehicle, containing organic solvents and organic binder only. In the second, a glass powder and an organic dispersing agent were also added.

All the organic components were decomposed after printing the films by an appropriate heat treatment. Table 1 shows the compositions of the two pastes before and after the heat treatment. For the second set of samples the grains of the pure $NiMn_2O_4$ source powder were covered with the commercial dispersing agent "Hypermer" (ICI Surfanctants, Hypermer LP1) using ethanol as a carrier liquid. The dispersing agent was dissolved in the ethanol and mixed thoroughly with the $NiMn_2O_{4+\delta}$ powder using an ultrasonic probe (KLN, 250/101). The ethanol was evaporated in the evacuated rotating evaporator.

The glass phase was included by mixing a glass powder (ESL Europe, code 428) to the Hypermer-covered $NiMn_2O_{4+\delta}$ grains.

Next, for both sets of samples the powder was dispersed in the vehicle (ESL Europe, type 403) using a petri dish and a spatula. Both types of pastes were further dispersed and possible agglomerates destroyed by ball milling (Otto Hermann, 2/7533).

The progress was monitored periodically by determining the size of major agglomerates with a grindometer (Simex, PF 50/2) until they were <10 μm.

The optimised pastes were then printed through a 115T-mesh polyester screen onto alumina substrates (CeramTec AG, thick film quality Rubalit 708) using a manual screen-printer (DEK, Model 240). The alumina substrates contained a glass phase ($\sim$4%), so strong bonding of film to substrates would occur if the printing paste and the resulting films also contain a glass phase.

The screen is the essential tool determining the thickness of the printed film.[9] The screen meshes serve as a volumetric vessel leading to predictable film thickness. After printing, the film thickness is reduced by the evaporation of the solvents and by the thermal treatment,

Table 1
Composition of the printing pastes

	Before thermal treatment/paste without glass (%)	After thermal treatment/paste without glass (%)	Before thermal treatment/paste with glass (%)	After thermal treatment/paste with glass (%)
Dispersing agent	–	–	0.85%	–
Glass	–	–	6.8%	8%
Vehicle	15%	–	15%	–
$NiMn_2O_4$ powder	85%	100%	77.35%	92%

but knowing the solid loading of the printing paste this shrinkage can be estimated.

For the screen-printing process the optimum distance between screen and substrate (snap off distance) was found empirically to be ~1.5 mm. The printing process was further optimised by varying the viscosity of the paste by adding different amounts of vehicle. The optimised values are given in Table 1. The optimum viscosity was ~10 Pa·s as determined using a viscosimeter (Paar Physica, UDS 200).

After printing, the organic components of the films were decomposed during an appropriate heat treatment and the films densified by an additional sintering procedure at 850 °C for 30 min.

The heat exposure for the heat treatment and the sintering procedure was again minimised in order to prevent extensive grain growth in the printed films, which leads to the formation of bigger grains merging together. This process leaves holes and pores on the film surface as the films only shrink in a direction perpendicular to the substrate, but hardly at all in the substrate plane during grain growth processes.

To minimise the heat exposure during decomposition of the organic vehicle components in the printed films thermal gravimetric analysis (TGA) for the pure vehicle was carried out to identify the temperature regions of the decomposition reactions. During the heat treatment of the printed films the temperature was increased much faster in temperature regions where such reactions were not taking place. The organic dispersing agent decomposed at similar temperatures to the organic additives in the vehicle and no further adjustment was necessary.

The heat exposure for the sintering process at 850 °C was minimised by varying the calcination time and testing the mechanical adhesion of the films to the substrate. A minimum sintering of 30 min at 850 °C was necessary to ensure phase purity. For the films with glass phase it was intended to achieve a reorientation of the particles by means of the glass, which exhibited a low viscosity at temperatures over 600 °C (liquid-phase-sintering).

The phase purity of the printed and fired films was assessed by XRD analysis, while the morphology was examined using scanning electron microscopy (Cambridge Instr., model S250 MK3) and laser profileometry (UBM Messtechnik).

3. Results and discussion

3.1. Powder processing

The thermal decomposition process of $NiMn_2(C_2O_4)_3{\cdot}6\ H_2O$, leading to $NiMn_2O_{4+\delta}$, was examined by thermal gravimetric analysis (TG). Fig. 2 shows the weight loss at a heating rate of 5 K per minute in air. The first three steps of the decomposition at 65 °C, 114 °C and 207 °C were interpreted as a stepwise release of residual adsorbed water and water of hydration. The reaction occurring at about 300 °C may well be the main decomposition of $NiMn_2(C_2O_4)_3$ into the precursor nickel and manganese oxides. The total weight loss during the release of water and the decomposition of the oxalate was 61% leading to an estimate for the chemical formula including residual adsorbed water and water of hydration of $NiMn_2(C_2O_4)_3{\cdot}9.1\ H_2O$.

The main reaction at 300 °C was found by DTA to be exothermic whereas the reactions assigned to the release of water proved to be endothermic. As mentioned before, the TGA data was used to minimise the heat exposure during calcining $NiMn_2(C_2O_4)_3{\cdot}9.1\ H_2O$, leading to $NiMn_2O_{4+\delta}$ with a small average grain size.

According to the phase diagram given by Wickham[8] the formation of $NiMn_2O_{4+\delta}$ starts to occur at temperatures above 750 °C. In Fig. 3 the XRD patterns for powders fired for 1 h at different temperatures are presented. These show that a minimum calcination temperature of 800 °C is necessary to gain phase pure $NiMn_2O_{4+\delta}$ by calcining for 1 h. For lower temperatures Mn_2O_3 traces are detectable.

In Figs. 4 and 5 the effect of the heat exposure on the grain size of the powder is demonstrated. In Fig. 4 the effect of increasing calcination temperature at constant calcination time (1 h) is shown whereas in Fig. 5 the temperature is constant (850 °C) and the calcination time altered.

In Fig. 4 the large increase of grain size at ~750 °C can be interpreted as the start of the formation of $NiMn_2O_{4+\delta}$. At higher temperatures the formation is complete and only a slight increase of grain size at higher temperature was observed. Conversely, the average grain size increased significantly and approximately linearly with increasing calcination time (Fig. 5). Therefore, priority was given to the reduction of the heating

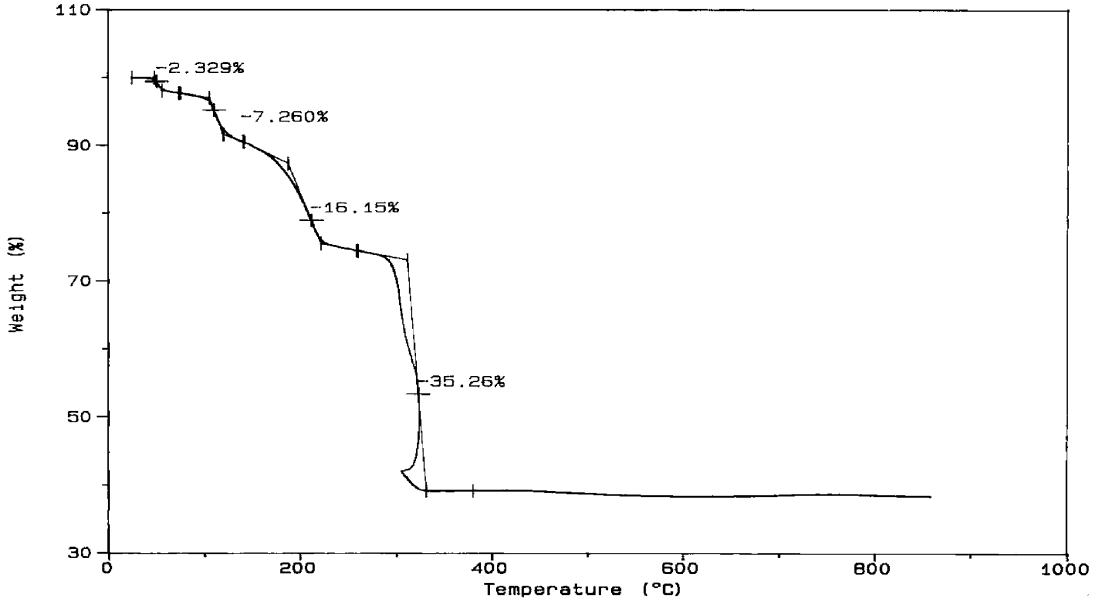

Fig. 2. Thermal gravimetry of $NiMn_2(C_2O_4)_3 \cdot x\ H_2O$; heating rate: 5 K/min in air.[5]

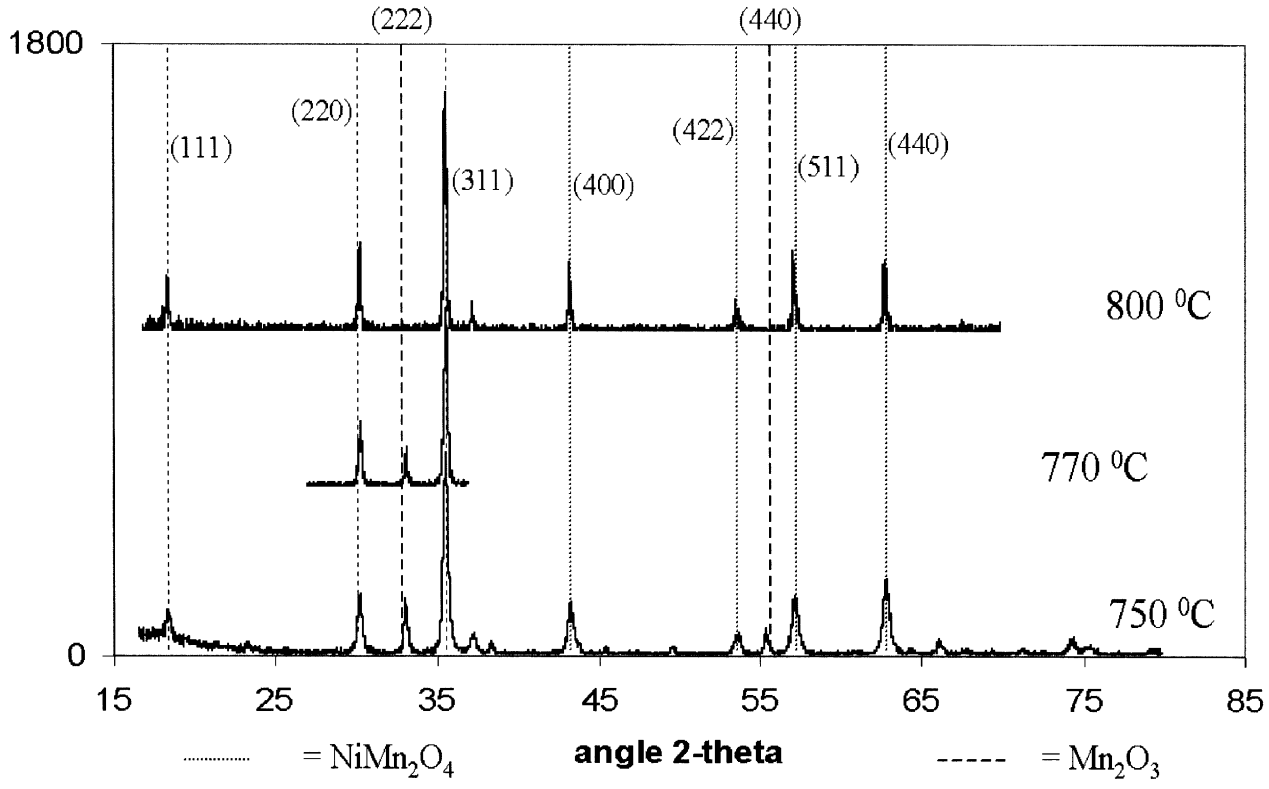

Fig. 3. XRD patterns for powders fired for 1 h at 750 °C, 770 °C and 800 °C.[5]

time. The minimum heat exposure leading to phase pure $NiMn_2O_{4+\delta}$ was found to be 30 min for a calcination process at 850 °C. The phase purity for this process was checked by XRD analysis. Although this is higher than the minimum temperature of 800 °C required to form $NiMn_2O_{4+\delta}$, it allowed a drastic reduction in heating time resulting in a small average grain size. By milling the powder the average grain size could be further reduced to <1 μm.

The powder stoichiometry was demonstrated to be correct using Inductive Coupled Plasma spectroscopy. Taking into account the inaccuracy in the ICP analysis the stoichiometry was found to be $Ni_{0.985\pm0.02}\ Mn_{2.015\pm0.02}\ O_{4+\delta}$ which is in the range of the desired $NiMn_2O_{4+\delta}$.

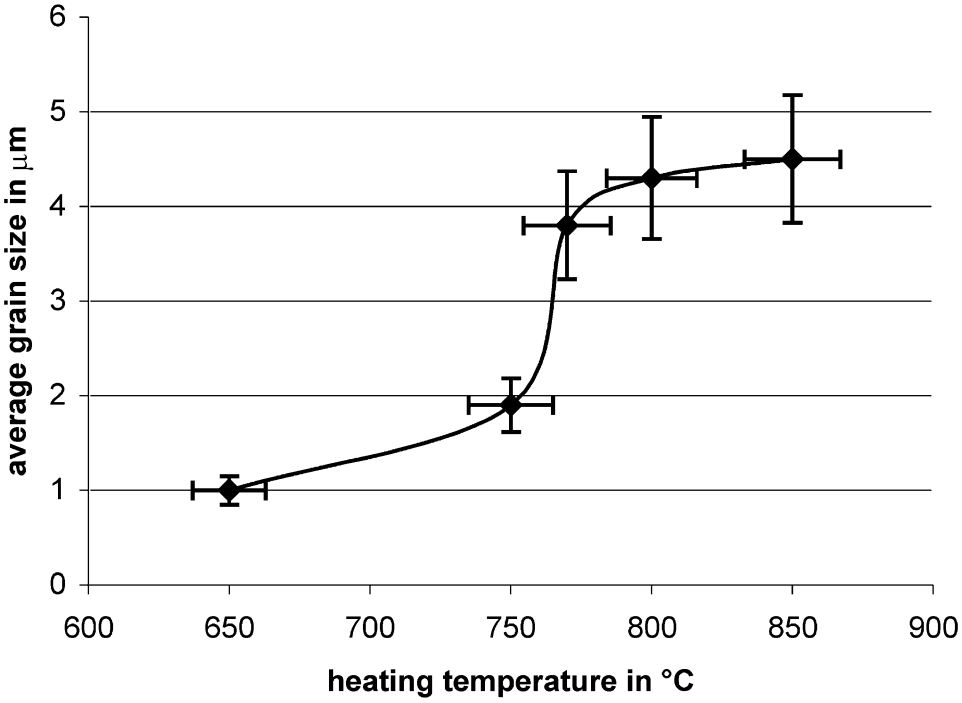

Fig. 4. Variation of average grain size with calcination temperature for 1 h.

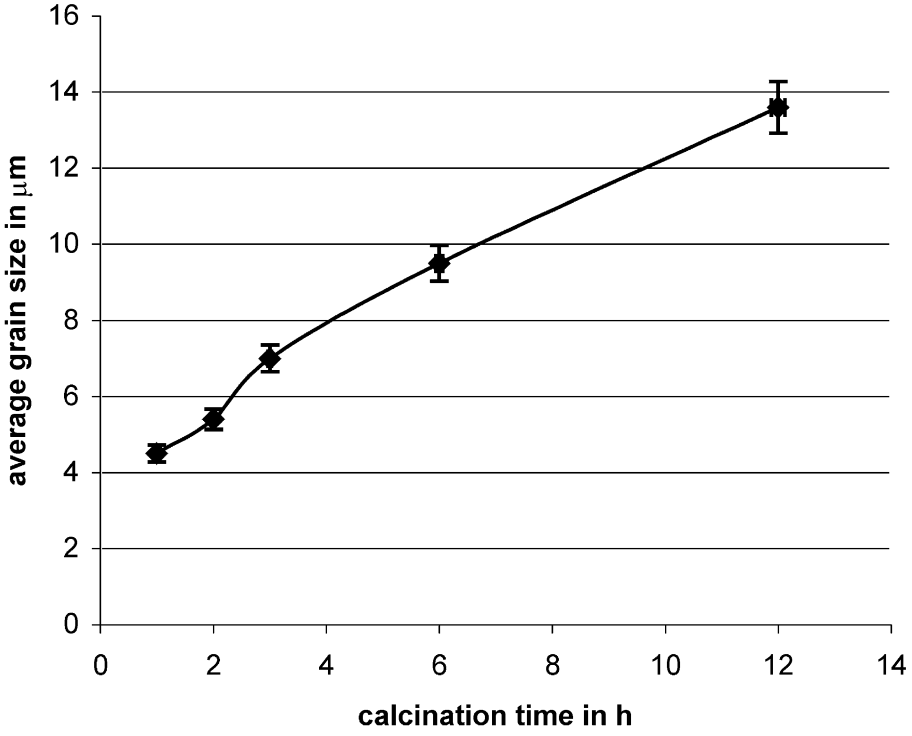

Fig. 5. Variation of average grain size with the calcination time at 850 °C.

3.2. Surface morphology of screen-printed films

The morphology of the screen-printed and fired films was assessed by scanning electron microscopy (SEM) and laser profileometry. The samples containing a glass phase and dispersing agent showed a denser and smoother surface with a lower average grain size. The SEM pictures given in Figs. 6 and 7 show the difference in the surface density and the average grain size clearly. From Fig. 6 it can be concluded that the glass phase

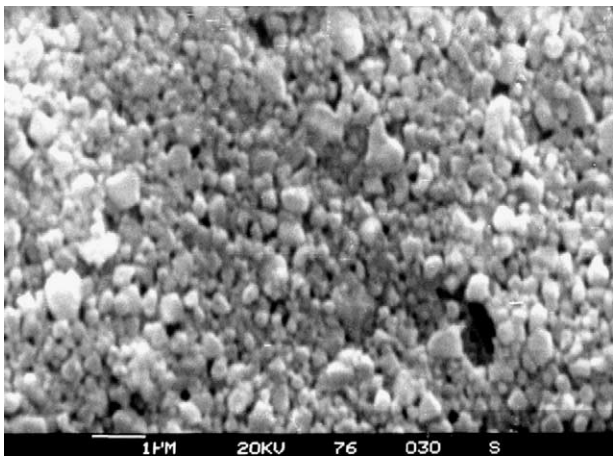

Fig. 6. SEM micrograph of a sintered surface (850 °C, 10 min, with glass phase; magnification: ×9000).

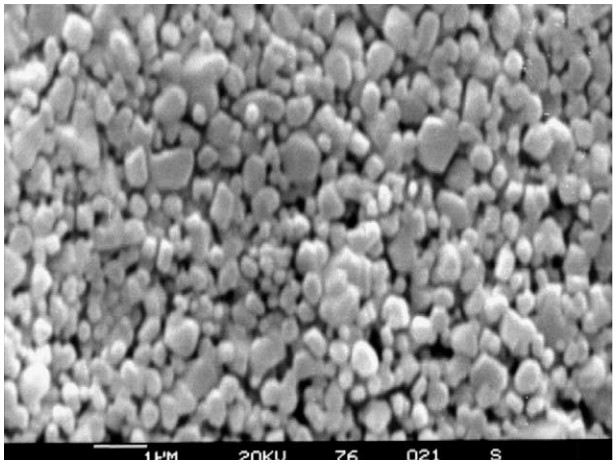

Fig. 7. SEM micrograph of a sintered surface (850 °C, 10 min, without glass phase; magnification: ×9000).

contracted the grains during the sintering process leading to a surface with fewer holes and pores. The glass exhibits a low viscosity at temperatures over 600 °C and liquid-phase-sintering occurs enabling a rearrangement of the grains. This is demonstrated in Figs. 8 and 9, which show the laser line scans over the surfaces of films prepared with and without glass phase. As can be seen, the surface of the glass containing film is much smoother.

Furthermore it could be shown that the film thickness of the glass containing sample was lower, indicating that the glass phase did result in an improvement of the particle packing as intended, leading to a denser film. The glass containing sample was about 25 µm thick, the one without glass ~30 µm.

It is clear from Figs. 6–9 that the addition of a glass phase provides a significant improvement in the surface topography.

However, it is believed that a more careful adjustment of the amount of glass powder added and an optimisation of the sintering procedure applied to the printed films could lead to even denser film surfaces further reducing the concentration of holes and pores visible in Fig. 6.

3.3. Phase purity of screen-printed films

The phase purity of the printed and fired films is demonstrated in the XRD spectra given in Fig. 10. It can be seen that for films, both with and without glass and dispersing agent, no peak was present which could not be assigned to either the $NiMn_2O_{4+\delta}$ or the Al_2O_3 substrate material. This is a strong indication for the phase purity of the fired films and it may be concluded that no chemical reactions between the $NiMn_2O_{4+\delta}$ source material, the glass phase or the substrate material had occurred.

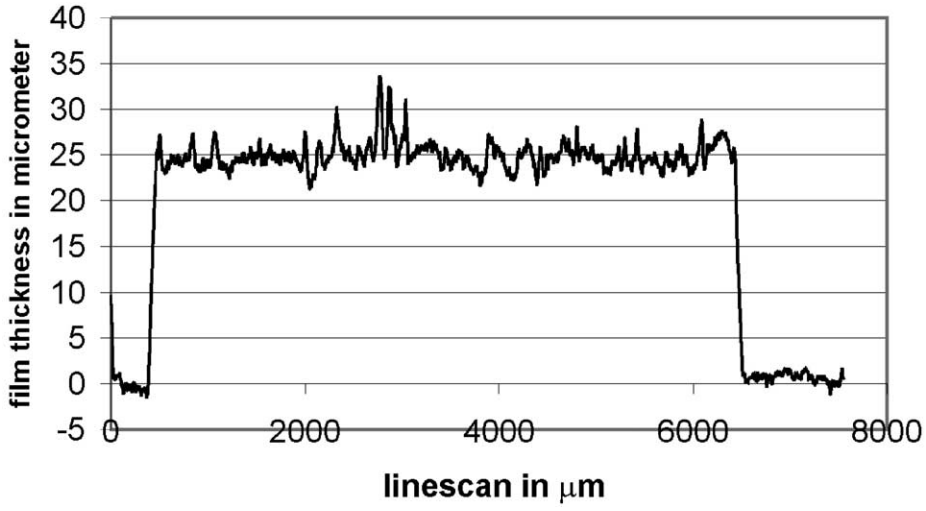

Fig. 8. Line scan for a sample with glass phase sintered at 850 °C for 30 min.

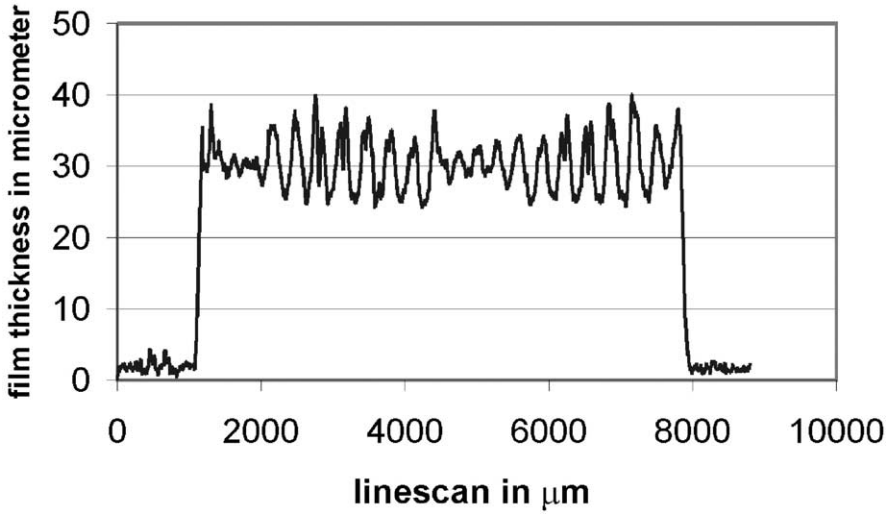

Fig. 9. Line scan for a sample without glass phase sintered at 850 °C for 30 min.

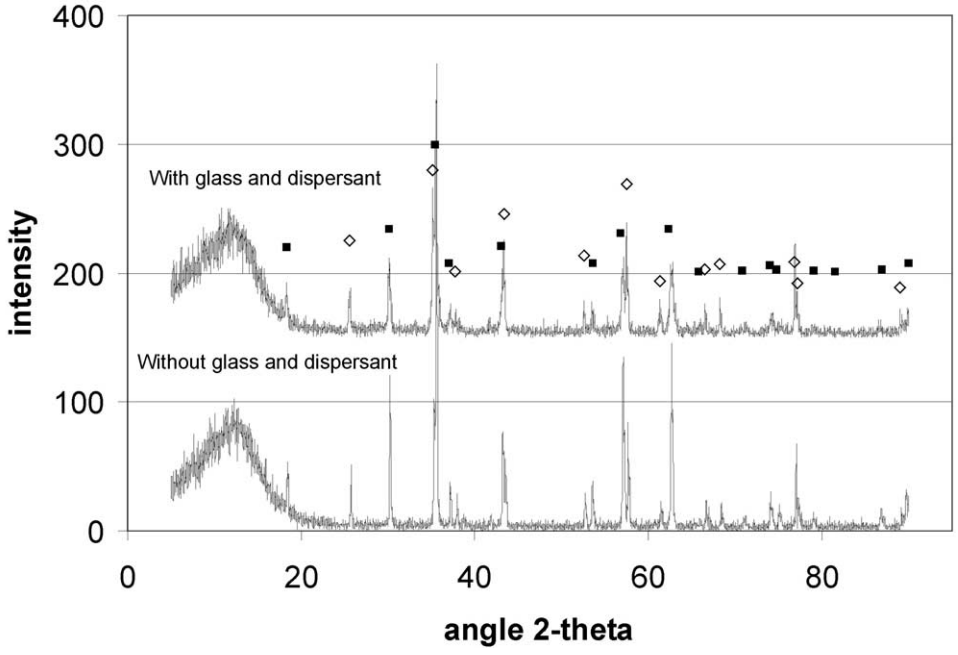

Fig. 10. X-ray spectra for films fired with and without glass phase and dispersant: ■ = $NiMn_2O_4$, □ = Al_2O_3 (substrate).

The films with dispersing agent showed slightly broader XRD peaks indicating a smaller average grain size as could be seen in the SEM micrographs.

3.4. Resistance vs. temperature characteristics

The R–T characteristics were measured at different temperatures in the range of 122–345 K. Two aluminium contacts were evaporated onto the films and covered by silver paint. Wires were attached with solder. The samples were placed in a liquid nitrogen cooled cryostat and computer controlled measurements were carried out. Fig. 11 shows typical NTCR characteristics for the two types of film: one printed using organic binders only and the other with the additional glass powder. The R–T characteristics in Fig. 11 were found to be well described by the variable-range-hopping model suggested by Efros and Shklovskii:[10]

$$R = R_0 T \exp(T_0/T)^{1/2} \quad (1)$$

R is the resistance, R_0 a constant, T the temperature and T_0 a characteristic temperature, determined by the slope of the $\ln(R \cdot T^{-1})$ vs. $(1/T)^{0.5}$ graph. Linear lines have been fitted through the data points and the slope been

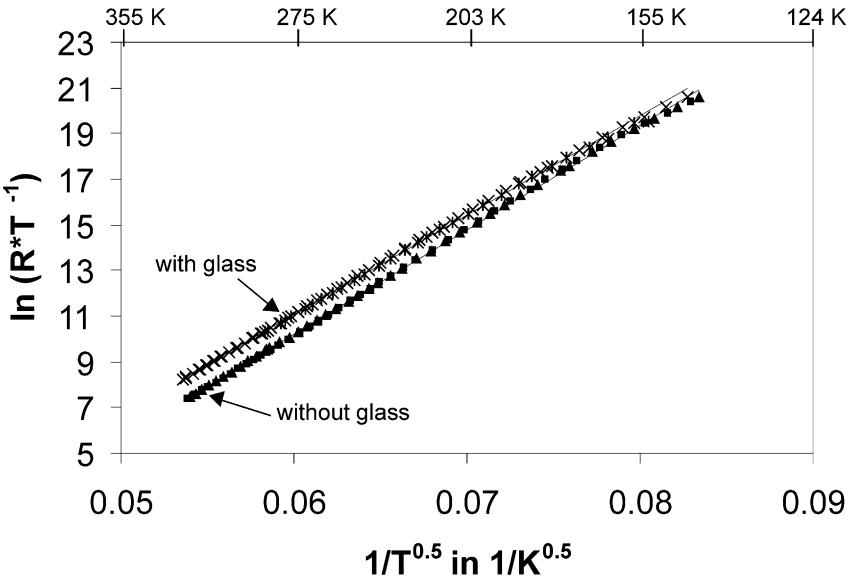

Fig. 11. $\ln(R \cdot T^{-1})$ vs. $(1/T)^{0.5}$ characteristic of fired $NiMn_2O_{4+\delta}$ films with and without glass.[5]

determined. Model (1) is based on the assumption that the electron hopping between Mn^{3+} and Mn^{4+} cations can be regarded as a conduction between localised electron states of varying energy and spatial separation (variable-range-hopping).[10] In this model it is assumed that the density of states is of parabolic shape, as opposed to the Mott [11] $(1/T)^{0.25}$ model for variable-range hopping, which is based on a uniform density of states. Recent tunnelling spectroscopy studies[12] have confirmed that the local density of states is indeed parabolic, justifying the use of Eq. (1). Nevertheless, the data was plotted against other axes, including Mott $(1/T)^{0.25}$, nearest-neighbour hopping $(1/T)$ and an empirical dependency:[13]

$$R = CT^{-4.83}\exp\left(\frac{T_0}{T}\right); \quad (2)$$

In none of these dependencies was the observed fit as good as that obtained with Eq. (1).

Fig. 11 also shows that the resistance was increased by the glass phase (factor of ~2) and that the slope of the graph, the characteristic temperature T_0, was decreased slightly from 1.95 to $2.11 \cdot 10^5$ K without glass to $1.82–1.92 \cdot 10^5$ K with glass. The good linearity of both curves indicated that the conduction mechanism was not affected by the glass phase and was consistent with the hopping model of Eq. (1).

This model was also suggested by Baliga and Jain investigating thin film NTCR ceramics,[14] although other authors have suggested nearest-neighbour hopping.[15]

The R–T characteristics presented in Fig. 11 were measured during both, heating and cooling cycles, but the resulting characteristics for both runs could hardly be resolved, indicating that for a given sample reproducibility was very good.

4. Conclusions

Thick films of $NiMn_2O_{4+\delta}$ displaying good NTCR characteristics have been produced by screen-printing, using either a paste with organic binders alone or with an additional glass phase and organic dispersing agent. In both types of film, the R–T characteristics were well described by a hopping model, although films incorporating the glass phase were slightly less temperature dependent. The glass containing films showed better surface properties and in general the addition of a glass phase can be regarded as a major improvement of the film quality. In order to produce an applicable temperature-sensing device more research is necessary to improve its performance under application conditions.

Acknowledgements

The authors wish to thank Prof. Dr. A. Feltz (Epcos AG, Deutschlandsberg, A) for the helpful discussion and suggestions concerning the powder preparation.

References

1. Brabers, V. A. M. and Terhell, J. C. J. M., *Phys. Stat. Sol. (a)*, 1982, **69**, 325–332.
2. Macklen, E. D., *Thermistors*. Electrochemical Publications, Glasgow, 1979.

3. Parlak, M., Hashemi, T., Hogan, M. J. and Brinkman, A. W., *J. Mater. Sci. Let.*, 1999, **17**, 1995.
4. Schmidt, R. and Brinkman, A. W., *International Journal of Inorganic Materials*, 2001, **3**(8), 1215–1217.
5. Schmidt, R., Stiegelschmitt, A., Roosen, A. and Brinkman, A. W., *Key Eng. Mater.*, 2002, **206-213**, 1417–1420.
6. Feltz, A. and Toepfer, J., *Z. Anorg. Allg. Chem.*, 1989, **576**, 71–80.
7. Feltz, A., Toepfer, J. and Schirrmeister, F., *J. Eur. Ceram. Soc.*, 1992, **9**, 187–191.
8. Wickham, D. G., *J. Inorg. Nucl. Chem.*, 1964, **26**, 1369–1377.
9. Franconville, F., Kurzweil, K. and Stalnecker, S. G., *Solid State Technology*, 1974, **Oct**, 61–68.
10. Efros, A. L. and Shklovskii, B. L., *J. Phys.*, 1975, **C8**, L49.
11. Mott, N. F. and Davis, E. A., *Electronic Processes in Non-Crystalline Materials*. Clarendon Press, Oxford, 1971.
12. Basu, A., Brinkman, A.W., Klusek, Z., Datta, P.K., Kowalczyk, P. *Journal of Applied Physics*, 2002, **92**, 4123–4125.
13. Becker, J. A., Green, C. B. and Pearson, G. L., *Bell Syst. Tech. J.*, 1947, **26**, 170.
14. Baliga, S. and Jain, A. L., *Materials Letters*, 1991, **11**(4–6), 226.
15. Lindner, F. and Feltz, A., *J. Eur. Ceram. Soc.*, 1993, **11**, 269.